



HAL
open science

How Spherical Are Gaseous Low Charged Dendrimer Ions: A Molecular Dynamics/Ion Mobility Study?

Fabrice Saintmont, Julien de Winter, Fabien Chirot, Emilie Halin, Philippe Dugourd, Patrick Brocorens, Pascal Gerbaux

► **To cite this version:**

Fabrice Saintmont, Julien de Winter, Fabien Chirot, Emilie Halin, Philippe Dugourd, et al.. How Spherical Are Gaseous Low Charged Dendrimer Ions: A Molecular Dynamics/Ion Mobility Study?. *Journal of The American Society for Mass Spectrometry*, 2020, 31 (8), pp.1673-1683. 10.1021/jasms.0c00113 . hal-02923341

HAL Id: hal-02923341

<https://hal.science/hal-02923341v1>

Submitted on 28 Oct 2020

HAL is a multi-disciplinary open access archive for the deposit and dissemination of scientific research documents, whether they are published or not. The documents may come from teaching and research institutions in France or abroad, or from public or private research centers.

L'archive ouverte pluridisciplinaire **HAL**, est destinée au dépôt et à la diffusion de documents scientifiques de niveau recherche, publiés ou non, émanant des établissements d'enseignement et de recherche français ou étrangers, des laboratoires publics ou privés.

How spherical are gaseous low charged dendrimer ions: a Molecular Dynamics / Ion Mobility study?

Fabrice Saintmont^{a,b}, Julien De Winter^a, Fabien Chiroc^c, Emilie Halin^a, Philippe Dugourd^d, Patrick Brocorens^b, Pascal Gerbaux^{a*}

^a Organic Synthesis & Mass Spectrometry Laboratory, Interdisciplinary Center for Mass Spectrometry (CISMa), Center of Innovation and Research in Materials and Polymers (CIRMAP), University of Mons - UMONS, 23 Place du Parc, 7000 Mons, Belgium

^b Laboratory for Chemistry of Novel Materials, Center of Innovation and Research in Materials and Polymers, Research Institute for Science and Engineering of Materials, University of Mons - UMONS, 23 Place du Parc, 7000 Mons, Belgium

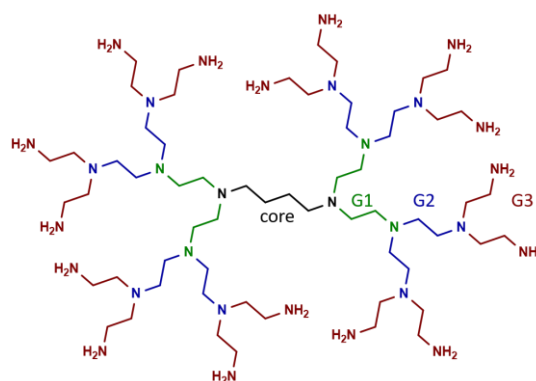
^c Univ Lyon, Université Claude Bernard Lyon 1, ENS de Lyon, CNRS, Institut des Sciences Analytiques, UMR 5280, 5 rue de la Doua, F-69100, Villeurbanne, France

^d Univ Lyon, Université Claude Bernard Lyon 1, CNRS, Institut Lumière Matière, F-69622, Lyon, France

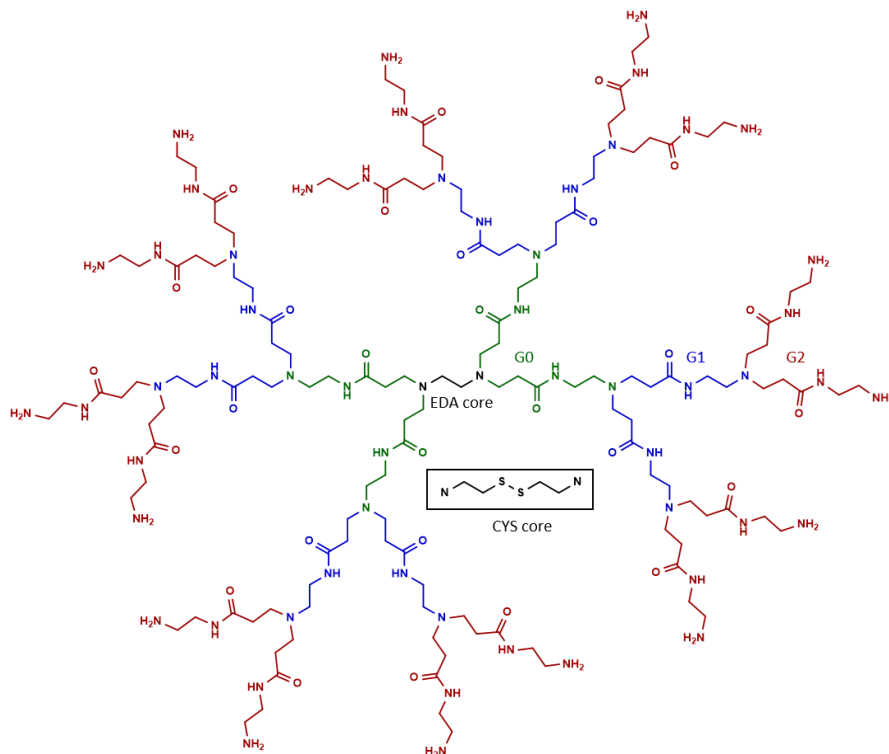
ABSTRACT: The globular shape of gaseous ions, resulting from the ionization of large molecules such as polymers and proteins, is a recurring subject that has undergone a renewed interest due to the advent of Ion Mobility Spectrometry (IMS), especially in conjunction with theoretical chemistry techniques such as Molecular Dynamics (MD). Globular conformations result from a fine balance between entropy and enthalpy considerations. For multiply charged ions isolated in the gas phase of a mass spectrometer, the coulombic repulsion between the different charges tends to prevent the ions from adopting a compact and folded 3D structure. In the present paper, we intimately associate data from IMS experiments and MD simulations to unambiguously access the conformations of dendrimer ions in the gas phase with a special attention paid to the dendrimer structure, the generation and the charge state. Doing so, we here combine a set of structural tools able to evaluate the (non)globular shape of ions based on both experimental and theoretical results.

INTRODUCTION

Dendrimers are hyperbranched polymers characterized by a well-defined structure. Their step-by-step synthesis allows a control of the molecular structure consisting of a central core and concentric layers of repeating units, which form branches. The layers are called generations (G) and dendrimers are labeled according to the number of generations they have. The most common dendrimers are poly(propylene imine) (PPI)¹ and poly(amidoamine) (PAMAM)² (Scheme 1 and 2).



Scheme 1: Structure of a poly(propylene imine) dendrimer of generation 3 with a dianinobutane core (black). The layers of generation 1 (green), 2 (blue) and 3 (red) are highlighted.



Scheme 2: Structure of a poly(amidoamine) dendrimer of generation 2 with an ethylene diamine core (EDA), or with a cystamine core (CYS) (see in the box). The layers of generation 0 (green), 1 (blue), and 2 (red) are highlighted. Note that generation 0 for PAMAM dendrimers corresponds to the generation 1 for PPI.

Amongst their numerous applications, PPI and PAMAM dendrimers are currently envisaged in medicine for drug and gene delivery, thanks to their biocompatibility and water solubility. They are proposed to act as cargo for small molecules by encapsulating hydrophobic drugs in their inner cavities³. Moreover, PAMAM and PPI dendrimers are polycationic at physiological pH and can interact electrostatically with polyanionic nucleic acids, forming supramolecular complexes called dendriplexes. Polycationic dendrimers can complex either plasmid DNA or short oligonucleotides and protect them from degradation by a nuclease. The global positive charge of the complex also enables interactions with the negatively charged cell membrane and the penetration of the membrane by endocytosis^{4,5}. Determining the structure of dendrimers in solution and its response to pH is thus of prime importance to understand and control the interactions of dendrimers with bioactive molecules^{6,7}.

In solution, dendrimers often adopt globular morphologies, and the influence of the generation, solvent, and pH conditions on the sphericity has been extensively documented^{6,8}. In their Molecular Dynamics (MD) investigation, Maiti *et al.* demonstrated that significant conformational changes occur in water upon pH modifications⁸. Low-pH conditions lead to a significant stretching of the dendrimer branches upon multiple amino group protonation. This size increase is

accompanied by a loss of sphericity compared to high- and neutral-pH cases⁸. The solvent molecules impact the 3D shape of the dendrimers by solvation, which reduces the intramolecular Coulomb repulsions between the protonated amino groups⁸.

These solvent effects disappear upon transfer of the protonated dendrimers to the gas phase in a mass spectrometer, for instance using Electrospray Ionization, and the dendrimer ions likely undergo conformational modifications to stabilize the ammonium groups. Ion Mobility Spectrometry in association with Mass Spectrometry (IMS-MS) is an analytical method that is nowadays extensively solicited to explore the 3-dimensional structures of gaseous (macro)ions. Structural information can be extracted from IMS-MS experiments based on the determination of Collision Cross Sections (CCS) of ions^{9,10}. Experimental CCS values are then compared to theoretical CCS, calculated using dedicated algorithms such as the Trajectory Method (TM) or the Projection Approximation (PA), for candidate structures generated by Molecular Dynamics (MD) simulations¹¹.

IMS-MS experiments on dendrimer ions are reported in the literature with a special emphasis on the influence of the charge state and the generation on the 3D structures of the macro-ions. Maire *et al.* analyzed PAMAM G0 to

G3 by IMS-MS and highlighted the increase of the CCS with the number of charges¹². In 2013, Tintaru *et al.* investigated two small PAMAM (G0-G1) dendrimers by IMS-MS and MD. They also detected a shape extension whose extent strongly depends on the PAMAM dendrimers architecture, *i.e.* globular or fan-shaped structure¹³. By MD calculations, they found that the conformational changes are dictated by electrostatic repulsion¹³.

Roughly spherical shape in the gas phase is a recurrent subject in ion mobility reports, since, for ideal spherical object, the CCS can be linked to the diameter of the ion, and thus to its molecular weight (MW) and/or its density. For instance, by plotting the evolution of the CCS with the MW for an extensive list of globular protein ions, Ruotolo *et al.* have shown that the best fit corresponds to a power relationship between the CCS and the MW, *i.e.* $CCS = 2.435 \times M^{2/3}$ ¹⁴. By approximating globular proteins as spheres, gas-phase densities of $0.36 \text{ Da}/\text{\AA}^3$ (0.60 g/cm^3)¹⁴⁻¹⁶ have been derived from experimental CCS. This value gives the upper limit for the density - estimated based on the CCS - of protein ions since globular protein ions may be considered as the most compact spatial arrangements for the peptide chains¹⁴. In other words, a blind estimation of the ion density based on the CCS is sometimes proposed as a criterion for globular proteins and densities lower than the determined upper limit are associated with extended/unfolded structures. However, the sphere approximation *inter alia* neglects the roughness of the protein ion surface and the roughness definitively contributes to the ion CCS and also somehow impacts the ion density.

In the present study, in order to shed some light on the relationship between ion structure, CCS, density and roughness, we investigate the evolution of the structures of gaseous dendrimer ions, as model ions, for increasing generation and charge state. We will pay a special attention to the correlation between the experimental CCS and the 3D structures of the MD simulated dendrimer ions, after assignment of the ion structures based on the comparison between the experimental and theoretical CCS. The identification of globular ions will be achieved by plotting the experimental CCS vs MW, allowing to calculate the gaseous ion density, which must be generation independent for dense roughly spherical ions. To approach the surface roughness that contributes to the CCS of the gaseous ions, the total area of the ion envelope can be theoretically estimated by determining the so-called Solvent-Accessible Surface Area (SASA)¹⁷, which can be obtained from MD data by considering helium as a solvent in the algorithm. In the present paper, for the identified globular ions, we will compare the CCS-derived geometrical data (ion surface, volume and density) with the MD data (SASA, effective ion volume and density), to highlight the geometrical character of the ion CCS.

PAMAM dendrimers G0 to G3 with two different cores, ethylene diamine (EDA) and cystamine (CYS) (Scheme 2), as well as PPI dendrimers from G1 to G3 (Scheme 1) are studied to monitor the influence of the nature of the repeating units, the nature of the core, the generation, and the charge state, on the gas phase structure and density of the dendrimer ions.

EXPERIMENTAL

Materials

CYS PAMAM G0 to G3 are synthesized according to Tomalia *et al.*¹⁸, with EDA PAMAM G0 and G1 present as synthesis impurities. EDA PAMAM G2 and G3 are obtained from Sigma Aldrich. PPI G1 to G3 are obtained from SyMO-Chem B.V., Eindhoven, The Netherlands.

Sample preparation

The dendrimer solutions are prepared at a concentration of approximately $50 \mu\text{M}$ in Milli-Q H_2O with 100mM ammonium acetate.

Collision cross section notation

The collision cross sections (CCS) will be abbreviated according to the accepted notation¹⁹. The notation is in the form ${}^X\text{CCS}_Y$, with X corresponding to the experimental/theoretical method used and Y the drift gas. In our case, the experimental CCS are written down as ${}^{\text{TW}}\text{CCS}_{\text{N}_2 \rightarrow \text{He}}$, corresponding to a measure using a Traveling Wave (TW) instrument filled with nitrogen gas, but calibrated using values obtained in helium. Values obtained on a Drift Tube (DT) filled with helium are written as ${}^{\text{DT}}\text{CCS}_{\text{He}}$. The theoretical CCS are in the form ${}^{\text{TM}}\text{CCS}_{\text{He}}$, corresponding to values calculated using the Trajectory Method (TM) with helium gas.

Mass spectrometry and Ion Mobility Spectrometry

MS spectra and CCS measurements are performed on a Waters Synapt G2-Si mass spectrometer. The solutions are infused at a flow rate of $5 \mu\text{l}/\text{min}$ with a capillary voltage of 2.5kV , a source temperature of 80°C and a desolvation temperature of 120°C . The ${}^{\text{TW}}\text{CCS}_{\text{N}_2 \rightarrow \text{He}}$ calibration is achieved according to the method developed by Duez *et al.*²⁰. The calibration is divided in two parts: (i) up to a CCS of 250 \AA^2 for small ions (PAMAM G0 and PPI G1) and (ii) above 250 \AA^2 for the other ions. The CCS are measured 5 times for small ions and 3 times for the other, with different ion mobility parameters listed in SI, to highlight that the CCS values are independent of those parameters. The ${}^{\text{TW}}\text{CCS}_{\text{N}_2 \rightarrow \text{He}}$ are compared to ${}^{\text{DT}}\text{CCS}_{\text{He}}$ ^{21,22} (see SI for experimental parameters, and Table S1 and S4 for values). The calibration in two parts presents lower deviation compared to the single calibration, especially for PAMAM G0 2+ and PPI G1 2+, having more than 13% of difference with the later. The ${}^{\text{TW}}\text{CCS}_{\text{N}_2 \rightarrow \text{He}}$ values are averaged on at least 3 measurements, with the associated errors being the standard deviation.

Molecular Dynamics

All dendrimers are built using LEaP tool from AMBER16^{23,24} with fragments from the Dendrimer Building Toolkit (DBT)²⁵. The CYS core is not available in the DBT but is created according to the same procedure. The different charge states are created by protonating selected primary amines to have the charges furthest from each other, to reduce their repulsive interactions. All the calculations are made using the gaff2 force field²⁶ in vacuum with an infinite cutoff.

The structures are submitted to 10 000 steps of energy minimization: 2 500 steps of steepest descent followed by 7 500 steps of conjugated gradient. The minimized structures are submitted to Langevin dynamics (NVT) with a collision frequency of 2 ps⁻¹. The time step is 2 fs with SHAKE constraints for bonds involving hydrogen. First, the structures are heated from 0 to 800 K during 5 ns, then cooled to 300K during 10 ns and equilibrated at 300K for 5 ns. The equilibration dynamics is carried out at 300K for 1 μ s. The dynamics is restarted until the distance RMSD remains constant over the last 1 μ s, the difference between the average RMSD of the first 500 ns and the last 500 ns being less than 0.1 Å. The constant RMSD and the low fluctuations of energies confirm that the system is equilibrated. The structures of each dendrimer shown in Figures (and in SI) are the last frame of the equilibrated dynamics. The TMCCS_{He} calculation is achieved by using 200 frames from the last 1 μ s of the production dynamics using Collidoscope²⁷. TMCCS_{He} values are the average on those 200 frames with the standard deviation as the error.

To characterize the structure of the ions, Radial Distribution Functions (RDF) are calculated between the geometrical center and all the atoms using the cptraaj module²⁸ on 2000 frames taken from the last 1 μ s of the production dynamics. The SASA with the respective molecular volume (V_{SASA}) are obtained on the last frame of the dynamics with Materials Studio 6.0 “Atom Volumes & Surfaces” module²⁹.

RESULTS AND DISCUSSION

1° Preparation of gaseous protonated PAMAM dendrimers

Aqueous solutions (100 mM ammonium acetate) of EDA (G2-G3) and CYS (G0-G3) PAMAM (~ 50 μ M) are analyzed using Electrospray Ionization (ESI) on a Waters Synapt G2-Si mass spectrometer (positive ion mode). Whatever the core and the generation, multi-charged ions are detected and correspond to $[M+nH]^{n+}$ ions, as featured in the ESI mass spectrum of CYS PAMAM G2 (Figure S1) and EDA PAMAM G2 (Figure S2), as typical examples. CYS PAMAM G2 ions appear from +2 to +6 charge states at m/z 1675, m/z 1117, m/z 838, m/z 670 and m/z 559, respectively, the most abundant ions being detected with 4 and 5 protons. CYS PAMAM G2, see Scheme 2, possesses 16 primary amine

groups available for protonation. Starting from the cystamine core, we can consider that G2 is characterized by 4 main branches (typically the branches created in G0), each bearing 4 terminal amino groups. Thus, for the +4 ions (m/z 838 in Figure S1), it is reasonable to propose that each main branch bears a proton, added on one of its amino group (see below).

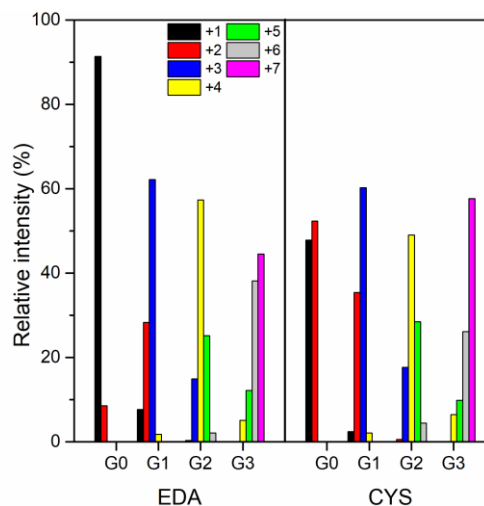


Figure 1: Electrospray mass spectrometry analysis of EDA and CYS PAMAM dendrimers: influence of the core and the generation on the charge distribution of the detected ions.

In Figure S1, signals related to EDA PAMAM G0 and G1 reflect the contamination of CYS PAMAM by EDA PAMAM impurities generated during the synthesis. These impurities are at least one generation lower than that of CYS PAMAM. The EDA PAMAM G1 ions are detected at m/z 1430, m/z 715, m/z 477 and m/z 358, respectively for the +1, +2, +3 and +4 ions.

As presented in Figure 1, for both analyzed PAMAM dendrimers, high generations tend to accept more protons than low generations, with a wider range of possible charge states: +1 and +2 for G0, +1 to +4 for G1, +2 to +6 for G2, and +4 to +7 for G3. For a given generation, the high charge states are more populated for CYS PAMAM than for EDA PAMAM, likely due to a better separation of the charges allowed with the longer cystamine core, $(R)_2N-CH_2-CH_2-S-S-CH_2-CH_2-N(R)_2$ vs $(R)_2N-CH_2-CH_2-N(R)_2$. This effect is significant for the small G0 dendrimer, where the maximum of the charge state distribution corresponds to +1 for EDA PAMAM and moves to +2 for CYS PAMAM; it is weaker for higher generations: the maximum of the charge state distributions corresponds to +3, +4 and +7 for G1 (8 primary amines), G2 (16), and G3 (32) dendrimers, respectively, irrespective of the core.

2° Experimental Collision Cross Sections (${}^{\text{TW}}\text{CCS}_{\text{N}_2 \rightarrow \text{He}}$) of PAMAM dendrimer ions

The ${}^{\text{TW}}\text{CCS}_{\text{N}_2 \rightarrow \text{He}}$ of the protonated dendrimers are measured using Traveling Wave Ion Mobility Spectrometry (TWIMS). For EDA PAMAM ions, our results can be compared to those of Maire *et al.* recorded in 2013, and we find that the CCS are in good agreement¹². For the sake of comparison and to validate our TWIMS calibration, we also measured the ${}^{\text{DT}}\text{CCS}_{\text{He}}$ (Table S1).

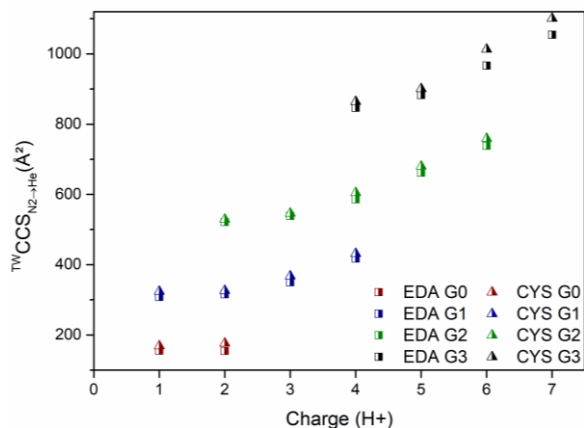


Figure 2: Evolution of the experimental ${}^{\text{TW}}\text{CCS}_{\text{N}_2 \rightarrow \text{He}}$ as a function of the charge state for EDA and CYS PAMAM from G0 to G3.

The ${}^{\text{TW}}\text{CCS}_{\text{N}_2 \rightarrow \text{He}}$ are reported in Figure 2, where we observe that both dendrimers, *i.e.* EDA core (square) vs CYS core (triangle), have similar CCS for a given generation and a given charge state, the CYS PAMAM ions having a slightly larger ${}^{\text{TW}}\text{CCS}_{\text{N}_2 \rightarrow \text{He}}$, attributed to the presence of additional atoms ($\text{C}_4\text{H}_8\text{S}_2$ vs C_2H_4) in the core.

We also observe that, for a given generation, the ${}^{\text{TW}}\text{CCS}_{\text{N}_2 \rightarrow \text{He}}$ remains constant up to a given number of charges, then globally increases with additional charges. Each ATD is monomodal and characterized by a quasi-constant resolution as presented in Figure S3 for the typical case of EDA G2. G0 only exists with two low-charge states, +1 and +2, both having a similar CCS determined around 160 \AA^2 . For G1, the ${}^{\text{TW}}\text{CCS}_{\text{N}_2 \rightarrow \text{He}}$ is similar for the two low-charged states, +1 and +2, *i.e.* G1 behaves as G0. But, two higher charge states also exist, where the CSS regularly increases with the charge. The same tendency is present in higher generations, except that the CCS plateau is shifted to higher charges: with G2 and G3, the ${}^{\text{TW}}\text{CCS}_{\text{N}_2 \rightarrow \text{He}}$ are constant for the +2/+3 and +4/+5 ions respectively, then increase regularly with the charge. The G0, G1, G2 and G3 dendrimers are thus able to respectively stabilize a maximum of two,

two, three and five charges without necessitating a structural expansion. The extension of the branches is assumed to be caused by coulombic repulsions no longer compensated by screening or any other self-solvation effects. However, these experimental values alone do not give any detailed information about the tridimensional structure of the ions. As the ${}^{\text{TW}}\text{CCS}_{\text{N}_2 \rightarrow \text{He}}$ does not change when the first charges are added, those ions are probably compact, and we can assume that they are roughly spherical. To confirm the sphere hypothesis, we study the evolution of the ${}^{\text{TW}}\text{CCS}_{\text{N}_2 \rightarrow \text{He}}$ vs the molecular mass of the ions, as proposed by Ruotolo *et al.* for globular protein ions¹⁴.

3° Spherical dendrimer ions: low charge states

Interestingly, the evolution of the CCS vs the mass (M) follows the expected trend for the growth of a spherical object (Equation 1), as already reported for roughly spherical protein ions¹⁴.

$$\text{CCS}_{\text{sph}} = A \times M^{2/3} \quad (1)$$

The power of 2/3 comes from the relation between the projected surface of a sphere, *i.e.* a disk, and its volume, and A is a fit constant equal to 2.435 for globular proteins¹⁴. This equation was applied by Maire *et al.* to EDA dendrimers to evaluate whether they organize as dense globules¹². However, while the exponent reflects the globular shape of the ion, the A coefficient reflects the ion density. Therefore, the correlation of the experimental CCS with this equation can only be made for proteins or substances with a similar density. As PAMAM is likely to have a different density than proteins, the A coefficient must be adjusted.

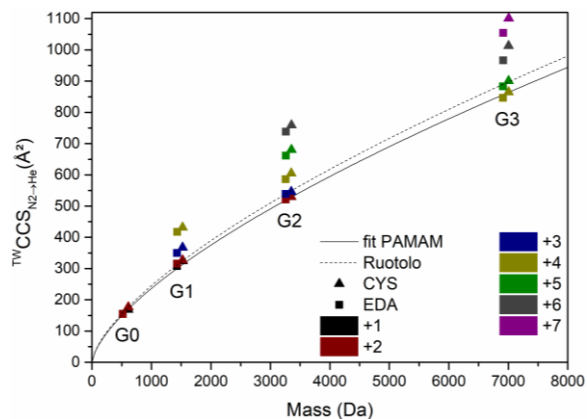


Figure 3: Evolution of ${}^{\text{TW}}\text{CCS}_{\text{N}_2 \rightarrow \text{He}}$ with the molecular mass of all charge state ions of EDA (square) and CYS (triangle) PAMAM. The plain curve corresponds to the fitted equation for the lowest charge states (Equation 2). The colors represent the charge state of the ions. The fit obtained by Ruotolo for protein ions is in dashed line for comparison¹⁴.

Figure 3 shows the evolution of the ${}^{\text{TW}}\text{CCS}_{\text{N}_2 \rightarrow \text{He}}$ for CYS and EDA PAMAM, as a function of the molecular weights. Assuming that the most compact structures of PAMAM, *i.e.* those with the lowest charge states, present negligible differences of density between the generations, they can be used to fit Equation 1. The CYS and EDA PAMAM G0 +1, G1 +1, G2 +2 and G3 +4 ions are used to build the fitted curve, which produces the following result:

$$\text{CCS}_{\text{sph}} = 2.37 \times M^{2/3} \quad (2)$$

As the EDA and CYS PAMAM G0 +1 and +2, G1 +1 and +2, G2 +2 and +3 and G3 +4 ions align on the fitted curve, they are considered roughly spherical. The 2.37 (± 0.01) value derived from the fitting is slightly lower than for a typical protein (2.435), showing that PAMAM dendrimer ions have a slightly higher density than protein ions. Dendrimer and polymer ions probably fold into more compact globules than protein ions due to the absence of the rigid structural features typical of proteins and the highest flexibility of the polymer/dendrimer chains^{30,31}.

Based on Equation 2, we can now probe the compactness of the other dendrimer ions by plotting the evolution of the ${}^{\text{TW}}\text{CCS}_{\text{N}_2 \rightarrow \text{He}}$ with the mass, the ions away from the fitted curve being more extended. The other charge states deviating from the fitted curve are thus either less dense, or less globular, or both. Globally, the core - EDA vs CYS - has no influence on the globular shape of the low-charge ions, as the same generations with the same charge states are on the fitted curve.

From Equation 2, it is possible to calculate the density (ρ_{CCS}) of the globular PAMAM ions by using Equation 3 with the implicit assumption that the PAMAM ions behave as spheres (see SI for the details of the Equation 2 to Equation 3 transformation).

$$\rho_{\text{CCS}} = \frac{3}{4} \sqrt{\frac{\pi}{2.37^3}} = 0.36 \text{ Da}/\text{\AA}^3 \quad (3)$$

A density of $0.36 \text{ Da}/\text{\AA}^3$ ($0.60 \text{ g}/\text{cm}^3$) is calculated for the globular PAMAM ions. This value is close to the density of globular protein ions, $0.35 \text{ Da}/\text{\AA}^3$ ($0.58 \text{ g}/\text{cm}^3$), calculated from Equation 1. This later value correlates with the densities of 0.35 and $0.36 \text{ Da}/\text{\AA}^3$ obtained by Kaddis and Bush, respectively, using Gas-phase Electrophoretic Mobility Molecular Analysis (GEMMA) for Kaddis, and ion mobility experiments on protein ions for Bush^{15,16}. Using Matrix-assisted Laser Desorption/Ionization (MALDI) MS and nanoelectrospray (nES) GEMMA data³², Müller *et al.* determined that spherical PAMAM dendrimers from G4 to G10 possess a constant average density of $0.39 \text{ Da}/\text{\AA}^3$ ($0.65 \text{ g}/\text{cm}^3$).

Assuming that the low charge state dendrimers are perfectly spherical, in addition to the apparent density, the radius, surface area, and volume can also be estimated.

As a typical example, the ions of EDA PAMAM G2 +2 are estimated to be spherical, see Figure 3. By associating those ions to spherical objects, the ${}^{\text{TW}}\text{CCS}_{\text{N}_2 \rightarrow \text{He}} = \text{CCS}_{\text{sph}}$ (521 \AA^2) can be considered as the projected surface area ($\pi \cdot R_{\text{CCS}}^2$) of a sphere whose area ($S_{\text{CCS}} = 4 \cdot \pi \cdot R_{\text{CCS}}^2$) is the total area of the ion envelope. For EDA PAMAM G2 +2 ions, $R_{\text{CCS}} = 12.88 \text{ \AA}$ is obtained and can also be injected in $V_{\text{CCS}} = \frac{4}{3} \cdot \pi \cdot R_{\text{CCS}}^3$ to calculate the corresponding solid sphere volume, $V_{\text{CCS}} = 8950 \text{ \AA}^3$.

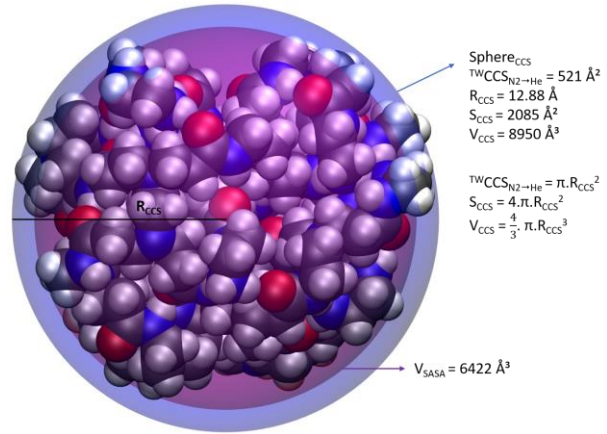


Figure 4: VDW representation of +2 EDA G2 with spheres representing the exact V_{CCS} (blue) and V_{SASA} (purple), see text. The 10% of difference between radii leads to 28% difference between volumes, affecting thereby the density estimation. For comparative purposes, the V_{SASA} is here assimilated to the volume of a sphere.

In Figure 4, the corresponding sphere is shown to nicely fit with the ion surface without reproducing it faithfully due to surface defects contributing to roughness. We may basically estimate that this sphere is surrounding the ion. Note that the ion structure in Figure 4 is obtained using Molecular Dynamics simulations as described in the next section of this paper.

The ratio between the MW of the ions and their V_{CCS} corresponds to the density previously calculated around $0.36 \text{ Da}/\text{\AA}^3$ based on Equation 3 derived from Figure 3.

The density defined by Equation 3 will be named ρ_{CCS} to specify that this density is calculated based on the CCS. All those parameters are gathered in Table 1 for all the lowest charge state dendrimer ions.

Table 1: Characteristics of lowest charge state PAMAM ions considered as spheres: Molecular Weight (MW); experimental collision cross section ($^{TW}CCS_{N_2 \rightarrow He}$); radius, surface and volume of a sphere having the same CCS; and density.

EDA PAMAM							
G_x	charge	MW (Da)	$^{TW}CCS_{N_2 \rightarrow He}$ (\AA^2)	R_{CCS} (\AA)	S_{CCS} (\AA^2)	V_{CCS} (\AA^3)	ρ_{CCS} ($\text{Da}/\text{\AA}^3$) ^a
G0	+1	517	155	7.03	621	1454	0.36
G1	+1	1430	308	9.90	1232	4064	0.35
G2	+2	3257	521	12.88	2085	8950	0.36
G3	+4	6912	847	16.42	3386	18528	0.37
CYS PAMAM							
G_x	charge	MW (Da)	$^{TW}CCS_{N_2 \rightarrow He}$ (\AA^2)	R_{CCS} (\AA)	S_{CCS} (\AA^2)	V_{CCS} (\AA^3)	ρ_{CCS} ($\text{Da}/\text{\AA}^3$) ^a
G0	+1	609	169	7.33	676	1653	0.37
G1	+1	1522	324	10.16	1296	4389	0.35
G2	+2	3350	529	12.98	2118	9163	0.37
G3	+4	7004	864	16.59	3458	19120	0.37
^a the CCS-based densities are calculated based on the $^{TW}CCS_{N_2 \rightarrow He}$							

4° Molecular modeling and theoretical CCS calculation

Using Molecular dynamics simulations with AMBER16 and the gaff2 force field, we optimize the structures of all the gaseous protonated dendrimers detected in the ESI experiments. The average $^{TM}CCS_{He}$ calculated across the dynamics are then compared with the $^{TW}CCS_{N_2 \rightarrow He}$ (see Figures 5 for EDA PAMAM and S4 for CYS). The theoretical CCS generally nicely agree with the experimental data, with differences being in average around 4% (Table S2). Nevertheless, several ions present huge differences between the experimental and the theoretical data. As a typical example, for EDA G1 +4, the ΔCCS amounts to 12.2 %, which is a value prohibitively too high to be of structural relevance. When compared to EDA G1 +3, we observe that the ΔCCS_{exp} and ΔCCS_{th} respectively amount to 16% and

7%. Despite repeated theoretical efforts, *i.e.* longer MD times, we are still not able to figure out the origin of these isolated discrepancies. Moreover, the $^{DT}CCS_{He}$ of those ions are not available as they are not detected. Except few exceptions, for the CYS counterparts, there is also a nice agreement between the experimental and the theoretical values.

Globally, we consider that the results in Table S2 validate the methodology used to model the dendrimer ions and we can assume that the tridimensional structures obtained theoretically for the dendrimers are close to the experimental ones, except for the isolated problematic cases. In our calculation, we also simulate the gas phase structures of the neutral dendrimers to evaluate the impact of the ionization on the dendrimer structure and we associate them with a $^{TM}CCS_{He}$.

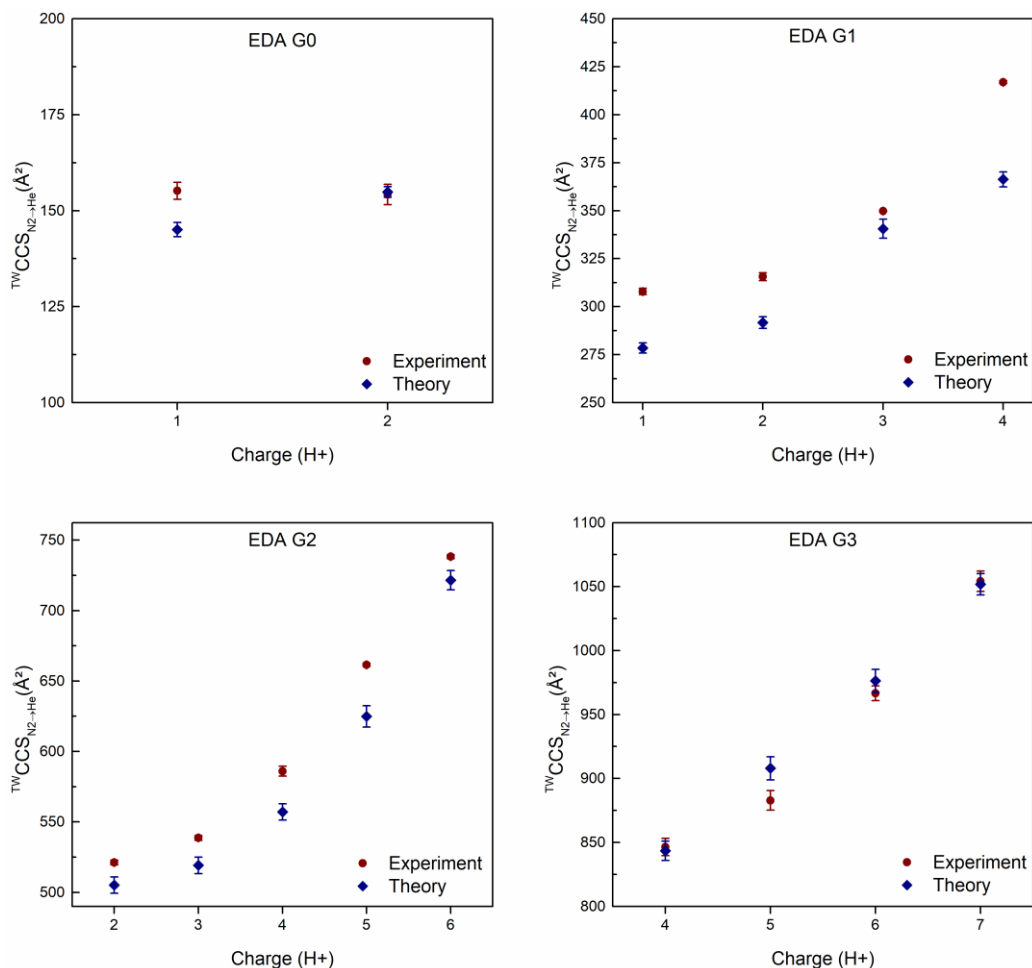


Figure 5: Comparison between experimental (red circle) and theoretical (blue diamond) CCS for EDA PAMAM G0 to G3. Error bars represent the standard deviation on 5 (G0) or 3 (G1 to G3) experimental measurements, and on 200 theoretical structures, respectively.

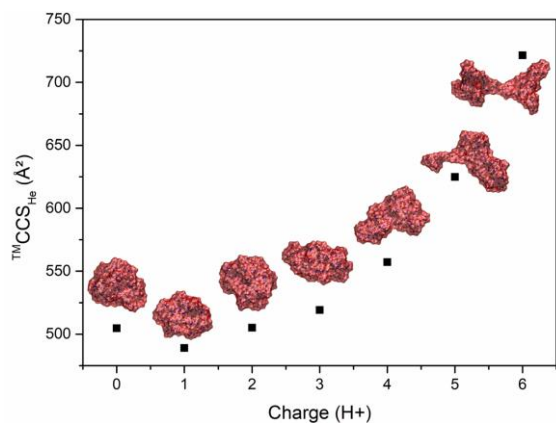


Figure 6: Evolution of the $TMCCS_{He}$ for EDA PAMAM G2 from 0 to 6 charges. For each charge state, the structure is represented with the vdW surface in red. (see text for the neutral dendrimer).

As an example, the structures and theoretical $TMCCS_{He}$ of all the EDA G2 ions and neutral are displayed in Figure 6. The neutral molecule and the singly- and doubly-charged ions present a globular shape with similar CCS, whereas the higher charge state ions are more and more extended, away from the globular structure. As featured in Figure 6, the addition of the first proton has a weak influence on the 3D structure, slightly decreasing the CCS. This slight compaction comes from the charge solvation effect, *i.e.* the local structuration of the molecule backbone around the charge. This is readily confirmed based on the examination of our MD structures, specifically the distribution of the electronegative carbonyl oxygen and amino nitrogen atoms around the ammonium group in the protonated dendrimer. Indeed, as shown in Figure S5, much more N/O atoms are present at short distances of the ammonium group than for any other amino group in the ion or in the neutral. We also observe that, in the ion, the average distribution of the N/O atoms around all the neutral amino terminal groups is shifted to smaller

distances when compared to the neutral dendrimer. This molecule structuration caused by charge solvation is clearly responsible for the ion compaction and reduced CCS. On the other hand, upon the stepwise addition of protons, we assist at a progressive elongation of the structure, which becomes ellipsoidal when reaching +3 charge state. For the +5 ions, the branches start to separate from each other, and reach a maximal separation for the +6 ions, which have a fully extended structure with the highest CCS. The same evolution is observed whatever the core and the generation (See Figures S6 to S12). Obviously, low generations require less charges than high generations to reach full extension, explaining why dendrimer ions of higher generations remain spherical over a broader range of charge states. Again, the impact of the core, EDA and CYS, is not significant, except for the G3 +7 ions, where the separation of the branches fully exposes the core to the surroundings in CYS PAMAM, while maintaining it buried in EDA PAMAM (See Figures S8 and S12).

5° Effective densities of the globular dendrimer ions

Based on the MD data, access to different structural parameters is granted and we can determine, for all the dendrimer ions and neutrals, their Solvent-Accessible Surface Area (SASA), along with the corresponding volume. For the present study, we use the helium atom as “solvent”, defined in the algorithm by its atomic radius, to ‘probe’ the surface of the dendrimers²⁹. This means that the SASA value includes also the contribution of the He atom, as an additional layer covering the ion surface. Except the small surface rugosities that are too small to be probed by the helium atom, the SASA considers the roughness of the surface. The volume delimited by the SASA, namely V_{SASA} , is accessible in the Materials Studio 6.0 “Atom Volumes & Surfaces” module and is used to estimate a new density, *i.e.* the ρ_{SASA} , to be compared with the density calculated based on the CCS values (ρ_{CCS}). Such a density is called the effective density since it better describes the mass-to-volume ratio. In Table S3, we gather all the molecular parameters that characterize the globular dendrimer ions (plus the neutrals). The SASA reasonably agree with the surface areas of the CCS-based sphere, say S_{CCS} , whose projected surface areas are the $^{TW}CCS_{N_2 \rightarrow He}$ (see Table 1 and Figure 4), with an average difference of ~4 %. This confirms the assumption that, for spherical objects, the $^{TW}CCS_{N_2 \rightarrow He}$ can be approximated as the projection of a sphere presenting a surface area equal to the effective surface of the ions. Whereas the SASA is marginally higher than the S_{CCS} , the theoretical V_{CCS} are higher than V_{SASA} (Figures 7 and S13). Therefore, the densities based on the V_{SASA} (ρ_{SASA}) are higher (0.39 to 0.55 Da/Å³) than the experimental or theoretical CCS-based densities (ρ_{CCS} ~0.36 Da/Å³ and 0.39 Da/Å³ respectively (Figures 7 and S13), the higher theoretical density coming from the smaller CCS, see Table S2). This is due to the more realistic volumes that are now considered as exemplified

in Figure 4. Indeed, the roughness of the ion increases the surface area compared to a sphere which would just encompass the ion, and the radius corresponding to this higher surface area leads to an overestimated sphere volume and so an underestimated CCS-based density.

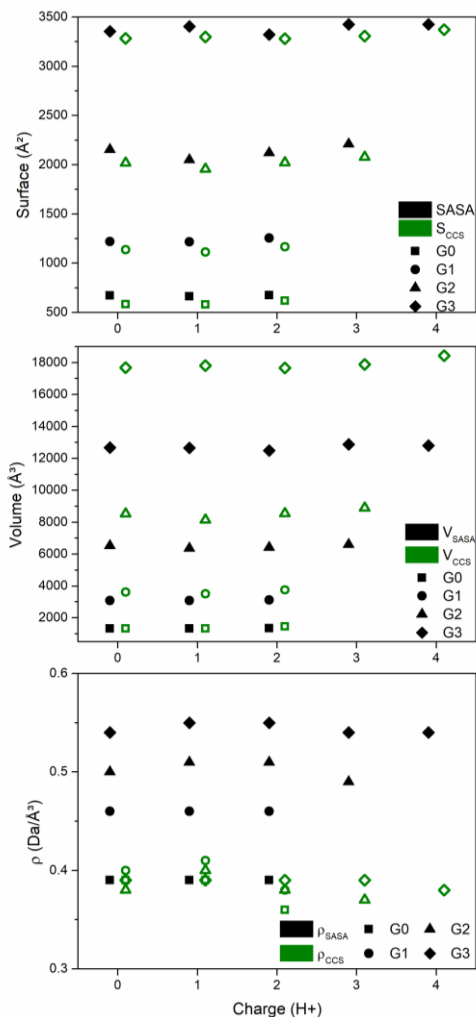


Figure 7: Comparison between surfaces (top), volumes (middle) and densities (bottom) from the last frame from the MD (black, solid) and calculated based on the average $^{TM}CCS_{He}$ on 200 frames (green, hollow) of EDA PAMAM ions and neutrals for G0 to G3.

Compared to the CCS-based density, which is constant over the generations, ρ_{SASA} increases with the generation, as the difference between the V_{CCS} and V_{SASA} increases with the generation. This is due to the decreasing impact of the extra volume defined by the He probe on the total volume - the SASA algorithm also includes the contribution of the He probe radius in the SASA volume - when increasing the size of the dendrimer (Figure S14). For a spherical dendrimer, this extra volume evolves as R^2 , while the molecular volume evolves as R^3 (see Figure S14).

From the confrontation between the CCS-derived geometrical data (S_{CCS} , V_{CCS} and ρ_{CCS}) and the MD data (SASA, V_{SASA} and ρ_{SASA}), it appears that the main pitfall in using the CCS of globular ions to obtain geometric information is the roughness of the surface of the ions. In the last section of this paper, we will monitor the evolution of the roughness of the gaseous ion surface by carrying out a layer-by-layer analysis of the ions starting from their geometric centers to determine the radial evolution of the number density.

6° Radial density of dendrimer ions

To evaluate the compactness of the dendrimer ions, concentric shells 0.1 Å thick are built around the geometric center of the ions (average of the positions of all the atoms). In each of these shells, the atoms are counted, and an averaged value is calculated on 2000 frames. Figure 8 presents the evolution of the number of atoms as a function of the distance from the geometrical center for 0 to +6 charge states of EDA G2 (see Figures S15-S21 for the other generations).

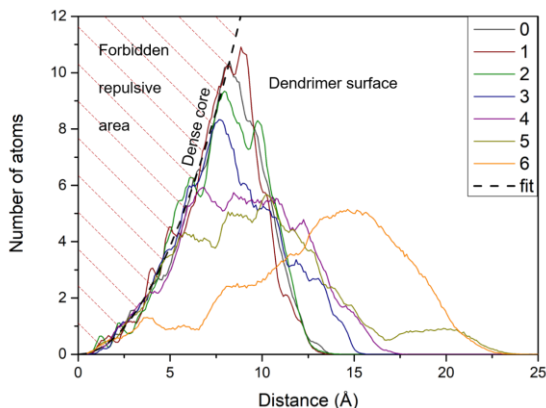


Figure 8: Number of atoms found in concentric shells 0.1 Å thick, as a function of the distance from the geometrical center. Results of EDA G2, for charge states 0 to +6. A parabolic fit corresponding to a dense core model is displayed in dashed lines.

For all the charge states, the number of atoms first increases, reaches a maximum, and then returns to zero. The position and the value of the maximum is observed to be charge state dependent. The highest maxima are measured for the neutral and the singly charged dendrimers around 8 Å from the geometrical center. With increasing charge state, the curves flatten with their maxima decreasing and moving to greater distances. The +5 and +6 ions are particularly extended with the distance reached by the most distant atoms close to 25 Å from the geometrical center. The growing part of all curves can be approached with a parabolic fitting. Such a parabolic increase is typical of homogeneous spheres, *i.e.* with a constant number density (n). In such a sphere, the number of atoms (N) in a shell situated at a distance

R from the center and thick by a ΔR value is given by Equation 4.

$$N(R \rightarrow R+\Delta R) = n V (R \rightarrow R+\Delta R) \quad (4)$$

Development of the Equation 4 can be found in SI and gives Equation 5 for $\Delta R = 0.1$ Å.

$$N(R \rightarrow R+\Delta R) = n 4\pi \left(0.1 R^2 + 0.01 R + \frac{0.001}{3} \right) \quad (5)$$

The increasing portions of the curves in Figure 8 can therefore be assimilated to a parabolic evolution, which makes it possible to calculate the number density (n). As seen in Figure 8, all the charge states have the same parabolic evolution of N ; the inner shells of these ions thus have the same density, which is the only adjustable parameter of Equation 5. The density is not only homogeneous within the inner core but is likely to be the maximum value due to a strong packing. The area on the left of the parabolic curves is thus forbidden by the van der Waals repulsive wall. The area on the right of the parabolic curves corresponds to shells where the packing of the atoms is sub-optimal, on average, since in these shells tightly packed and empty domains coexist. The curves in Figure 8 follow the parabolic evolution of maximal packing up to a given distance, then enter the sub-optimal packing area, where they decline to zero. The parabolic evolution corresponds to the dense core of the dendrimer and the decrease corresponds to the surface. What is called a surface is thus characterized by a thickness and is best described as perforated outer shells, contributing to the roughness of the dendrimer ion surface. The surface appears at a shorter distance from the core when the number of charges increases; for the +6 charge state, the parabolic increase is negligible (2.5 Å is on the order of a H...H van der Waals contact), showing that the corresponding ions have no dense core. There are few atoms near the center; most of them are located far from it, resulting in the structure shown in Figure 6 with branches extended from either side of the core. By fitting the parabolic increase of the curves with Equation 5, we can obtain the constant number density (n) of the dense core. The data to fit must be taken up to the apex of the curves. Rather than localizing arbitrarily the apex, the fit is made by increasing progressively the number of data³³. Then, the fit with the lowest error is retained. The number densities are extracted for each generation and each charge state and displayed in Figure 9.

Most number densities are around 0.12 atoms/Å³ for both cores (EDA and CYS). Deviating densities occur for systems where a small number of data is available to fit, because the parabolic part of the curve is of limited extension. The average number densities are then calculated for each core using the values between 0.10 atoms/Å³ and 0.14 atoms/Å³ in Figure 9, giving 0.12 atoms/Å³ for both cores, and are represented on Figure 9. These values are close to each other, so the number

density of the center does not depend on the nature of the core – EDA vs CYS - with an average of 0.12 atoms/Å³ for PAMAM, this average value is used to build the parabolic model of Figure 8. This number density can be compared with number densities of approximately 0.09 atoms/Å³ obtained by Maiti *et al.* for EDA PAMAM in the gas phase³⁴. The lower densities obtained by Maiti *et al.* compared to ours can be explained by the force field used in their work. Indeed, they used the Dreiding force field which is known to generally underestimate the densities³⁵.

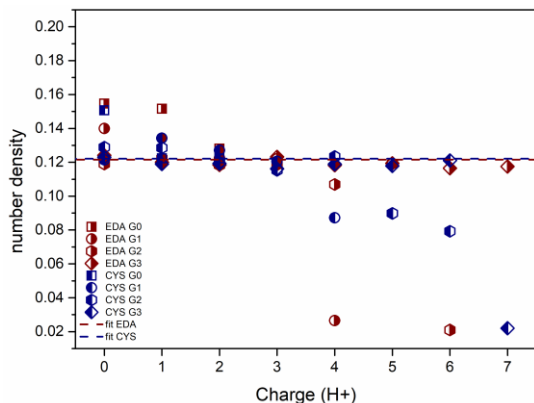


Figure 9: Number densities of the dense core for EDA (right filled) and CYS PAMAM (left filled) G0 to G3 with different charge states. The average densities for both cores are represented in dash lines.

7° PPI dendrimer

All the analysis above are also made for PPI ions and the main differences are summarized here. The ${}^{\text{TW}}\text{CCS}_{\text{N}_2 \rightarrow \text{He}}$ of PPI ions from G1 to G3 are measured and represented in Figure S22. Similar to the PAMAM case, the evolution of the CCS with the mass of the lowest charge state ions can be fitted with $\text{CCS} = A \times M^{2/3}$ (Equation 6 in Figure 10). For PPI, the A coefficient is higher than for PAMAM (2.68 vs 2.37), giving a smaller density of 0.30 Da/Å³ (0.50 g/cm³) (vs 0.36 Da/Å³ for PAMAM). The smaller density is consistent with the fact that PPI contain only hydrogen, carbon and nitrogen atoms, while PAMAM also contains heavier oxygen atoms. By comparing the ${}^{\text{TW}}\text{CCS}_{\text{N}_2 \rightarrow \text{He}}$ of all the detected PPI ions with the CCS obtained by Equation 6, it appears that only the lowest charge state ions are spherical, PPI being unable to stabilise more than one or two charges for the generations studied. The densities (ρ_{CCS} and ρ_{SASA}) of the lowest charge states are listed in Table S6.

The ${}^{\text{TM}}\text{CCS}_{\text{He}}$ calculated on the theoretical structures are then compared to the ${}^{\text{TW}}\text{CCS}_{\text{N}_2 \rightarrow \text{He}}$, with a difference between 0.4 and 5.7 % (Table S5 and Figure S23-25). The evolution of the ${}^{\text{TM}}\text{CCS}_{\text{He}}$ with the charge for the neutral and ions, and the radial distribution of atoms are in SI (Figure S26-S31). From the radial distributions, the PPI dense core is characterized by an average number density (Figure S32) of 0.13 atoms/Å³ (vs 0.12 atoms/Å³

for PAMAM). Therefore, PPI core is more densely packed than PAMAM core, but the lack of oxygen atoms leads to a smaller mass density.

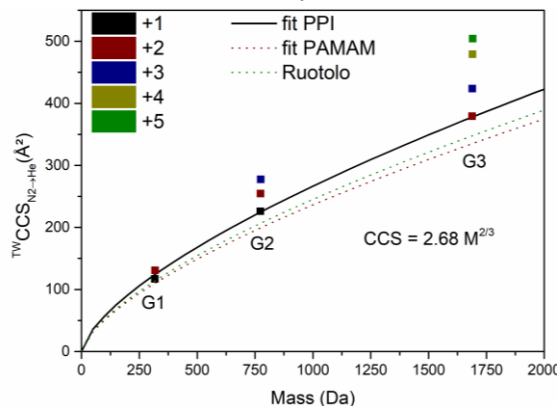


Figure 10: Evolution of ${}^{\text{TW}}\text{CCS}_{\text{N}_2 \rightarrow \text{He}}$ with the molecular mass of the lowest charge state PPI ions. The colors indicate the charge state. The fits obtained by Ruotolo for protein ions and ours for PAMAM are in dotted lines for comparison.

CONCLUSIONS

In this study, we measured the ${}^{\text{TW}}\text{CCS}_{\text{N}_2 \rightarrow \text{He}}$ of PAMAM G0 to G3 with EDA and CYS as the core, and of PPI G1 to G3. The increase of the CCS with the number of charges leads to the expansion of the structure caused by coulombic repulsion. The globular shape of ions can be estimated using a purely geometrical model considering the ions as spheres. That model allows to estimate, based on the CCS, an ion density (ρ_{CCS}), with PAMAM being close to proteins, 0.36 Da/Å³ and 0.35 Da/Å³ respectively, while PPI have a smaller density of 0.30 Da/Å³ due to its chemical composition. Using Molecular Dynamics simulations, we visually analyzed the evolution of the ion shape for the different generations and increasing charge states. The MD data demonstrate that the CCS-based predictions for globular shape is reliable. For roughly spherical ions, the CCS is often approximated as the projection of a sphere presenting a surface area equal to the effective surface of the ions. This is confirmed in the present study by correlating the surface area of the CCS-base sphere with the Solvent-Accessible Surface Area (SASA) that is calculated starting from the MD structures. The volume delimited by the SASA was thus used to estimate a new density that is shown to be higher than the CCS-based density, due to the more realistic volumes considered. Nevertheless, such a density calculation was also shown to be biased due to the presence of the probe during the determination of the SASA. From the confrontation between the CCS-derived and MD geometrical data, the main pitfall in using the CCS of roughly spherical ions to obtain geometric information is confirmed to be the ion surface roughness. Using Molecular Dynamics simulations, we finally highlighted that, except for

higher charge states, gaseous dendrimer ions present a dense core with a number density specific to the nature of the dendrimer. PPI ions are slightly more packed than PAMAM ions, 0.13 atoms/Å³ and 0.12 atoms/Å³ respectively.

All those tools and parameters can be useful to characterize the structure, and moreover the globular shape, of ions studied by Ion Mobility Spectrometry.

As a perspective, the good agreement with ^{DT}CCS_{He} and the robustness of the structure make those dendrimers suitable to be used as CCS calibrants.

Acknowledgments

The MS lab is grateful to the “Fonds National de la Recherche Scientifique (FRS-FNRS)” for financial support for the acquisition of the Waters Synapt G2-Si mass spectrometer and to the UMONS for the PhD grant of Fabrice Saintmont. Computational resources have been provided by the Consortium des Équipements de Calcul Intensif (CÉCI), funded by the Fonds de la Recherche Scientifique de Belgique (F.R.S.-FNRS) under Grant No. 2.5020.11 and by the Walloon Region.

SUPPORTING INFORMATION

CCS comparison, MS spectra, evolution of CCS with charge state, RDF, equation development, IMS parameters.

REFERENCES

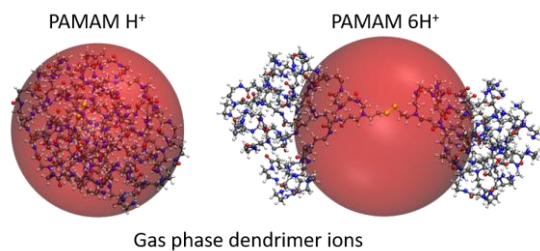
- Buhleier, E.; Wehner, W.; Vögtle, F. “Cascade”- and “Nonskid-Chain-like” Syntheses of Molecular Cavity Topologies. *Synthesis (Stuttg)*. **1978**, *1978* (02), 155–158.
- Tomalia, D. A.; Baker, H.; Dewald, J.; Hall, M.; Kallos, G.; Martin, S.; Roeck, J.; Ryder, J.; Smith, P. A New Class of Polymers: Starburst-Dendritic Macromolecules. *Polym. J.* **1985**, *17* (1), 117–132.
- Caminade, A.-M.; Turrin, C.-O. Dendrimers for Drug Delivery. *J. Mater. Chem. B* **2014**, *2* (26), 4055.
- Eichman, J. D.; Bielinska, A. U.; Kukowska-Latallo, J. F.; Baker, J. R. The Use of PAMAM Dendrimers in the Efficient Transfer of Genetic Material into Cells. *Pharm. Sci. Technol. Today* **2000**, *3* (7), 232–245.
- Dufès, C.; Uchegbu, I. F.; Schätzlein, A. G. Dendrimers in Gene Delivery. *Adv. Drug Deliv. Rev.* **2005**, *57* (15), 2177–2202.
- Lee, K.-H.; Lee, I.; Baker, J. R.; Banaszak Holl, M. M. Effect of PH and Generation on Structural Properties of Poly(Amidoamine) Dendrons Studied by Molecular Dynamics Simulations. *J. Comput. Theor. Nanosci.* **2012**, *9* (1), 127–136.
- Lombardo, D. Modeling Dendrimers Charge Interaction in Solution: Relevance in Biosystems. *Biochem. Res. Int.* **2014**, *2014*, 1–10.
- Maiti, P. K.; Çağın, T.; Lin, S. T.; Goddard, W. A.; Cagin, T.; Lin, S. T.; Goddard, W. A. Effect of Solvent and PH on the Structure of PAMAM Dendrimers. *Macromolecules* **2005**, *38* (3), 979–991.
- McDaniel, E. W.; Martin, D. W.; Barnes, W. S. Drift Tube-Mass Spectrometer for Studies of Low-Energy Ion-Molecule Reactions. *Rev. Sci. Instrum.* **1962**, *33* (1), 2–7.
- Smith, D. P.; Knapman, T. W.; Campuzano, I.; Malham, R. W.; Beryman, J. T.; Radford, S. E.; Ashcroft, A. E. Deciphering Drift Time Measurements from Travelling Wave Ion Mobility Spectrometry-Mass Spectrometry Studies. *Eur. J. Mass Spectrom. (Chichester, Eng)*. **2009**, *15* (2), 113–130.
- D’Atri, V.; Porrini, M.; Rosu, F.; Gabelica, V. Linking Molecular Models with Ion Mobility Experiments. Illustration with a Rigid Nucleic Acid Structure. *J. Mass Spectrom.* **2015**, *50* (5), 711–726.
- Maire, F.; Coadou, G.; Cravello, L.; Lange, C. M. Traveling Wave Ion Mobility Mass Spectrometry Study of Low Generation Polyamidoamine Dendrimers. *J. Am. Soc. Mass Spectrom.* **2013**, *24* (2), 238–248.
- Tintaru, A.; Priel, S.; Denbigh, L.; Liu, X.; Peng, L.; Charles, L. Conformational Changes of Small PAMAM Dendrimers as a Function of Their Charge State: A Combined Electrospray Mass Spectrometry, Traveling-Wave Ion Mobility and Molecular Modeling Study. *Int. J. Mass Spectrom.* **2013**, *354–355*, 235–241.
- Ruotolo, B. T.; Benesch, J. L. P.; Sandercock, A. M.; Hyung, S.-J.; Robinson, C. V. Ion Mobility–Mass Spectrometry Analysis of Large Protein Complexes. *Nat. Protoc.* **2008**, *3* (7), 1139–1152.
- Bush, M. F.; Hall, Z.; Giles, K.; Hoyes, J.; Robinson, C. V.; Ruotolo, B. T. Collision Cross Sections of Proteins and Their Complexes: A Calibration Framework and Database for Gas-Phase Structural Biology. *Anal. Chem.* **2010**, *82* (22), 9557–9565.
- Kaddis, C. S.; Lomeli, S. H.; Yin, S.; Berhane, B.; Apostol, M. I.; Kickhoefer, V. A.; Rome, L. H.; Loo, J. A. Sizing Large Proteins and Protein Complexes by Electrospray Ionization Mass Spectrometry and Ion Mobility. *J. Am. Soc. Mass Spectrom.* **2007**, *18* (7), 1206–1216.
- Lee, B.; Richards, F. M. The Interpretation of Protein Structures: Estimation of Static Accessibility. *J. Mol. Biol.* **1971**, *55* (3).
- Tomalia, D. A.; Huang, B.; Swanson, D. R.; Brothers, H. M.; Klimash, J. W. Structure Control within Poly(Amidoamine) Dendrimers: Size, Shape and Regio-Chemical Mimicry of Globular Proteins. *Tetrahedron* **2003**, *59* (22), 3799–3813.
- Gabelica, V.; Shvartsburg, A. A.; Afonso, C.; Barran, P.; Benesch, J. L. P.; Bleiholder, C.; Bowers, M. T.; Bilbao, A.; Bush, M. F.; Campbell, J. L.; Campuzano, I. D. G.; Causon, T.; Clowers, B. H.; Creaser, C. S.; De Pauw, E.; Far, J.; Fernandez-Lima, F.; Fjeldsted, J. C.; Giles, K.; Groessl, M.; Hogan, C. J.; Hann, S.; Kim, H. I.; Kurulugama, R. T.; May, J. C.; McLean, J. A.; Pagel, K.; Richardson, K.; Ridgeway, M. E.; Rosu, F.; Sobott, F.; Thalassinou, K.; Valentine, S. J.; Wyttenbach, T. Recommendations for Reporting Ion Mobility Mass Spectrometry Measurements. *Mass Spectrom. Rev.* **2019**, *38* (3), 291–320.
- Duez, Q.; Chirot, F.; Liénard, R.; Josse, T.; Choi, C.; Coulembier, O.; Dugourd, P.; Cornil, J.; Gerbaux, P.; De Winter, J. Polymers for Traveling Wave Ion Mobility Spectrometry Calibration. *J. Am. Soc. Mass Spectrom.* **2017**, *28* (11), 2483–2491.
- Simon, A. L.; Chirot, F.; Choi, C. M.; Clavier, C.; Barbaire, M.; Maurelli, J.; Dagany, X.; MacAleese, L.; Dugourd, P. Tandem Ion Mobility Spectrometry Coupled to Laser Excitation. *Rev. Sci. Instrum.* **2015**, *86* (9).
- Choi, C. M.; Simon, A.; Chirot, F.; Kulesza, A.; Knight, G.; Daly, S.; MacAleese, L.; Antoine, R.; Dugourd, P. Charge, Color, and Conformation: Spectroscopy on Isomer-Selected Peptide Ions. *J. Phys. Chem. B* **2016**, *120* (4), 709–714.
- Case, D. A.; Betz, R. M.; Cerutti, D. S.; Cheatham III, T. E.; Darden, T. A.; Duke, R. E.; Giese, T. J.; Gohlke, H.; Goetz, A. W.; Homeyer, N.; Izadi, S.; Janowski, P.;

- Kaus, J.; Kovalenko, A.; Lee, T. S.; LeGrand, S.; Li, P.; Lin, C.; Liu, J.; Luchko, T.; Luo, R.; Madej, B.; Mermelstein, D.; Merz, K. M.; Monard, G.; Nguyen, H.; Nguyen, H. T.; Omelyan, I.; Onufriev, A.; Roe, D. R.; Roitberg, A.; Sagui, C.; Simmerling, C.; Botello-Smith, W. M.; Swails, J.; Walker, R. C.; Wang, J.; Wolf, R. M.; Wu, X.; Xiao, L.; Kollman, P. A. Amber 2016. *University of California, San Francisco*. 2016.
- (24) Wang, J.; Wang, W.; Kollman, P. A.; Case, D. A. Automatic Atom Type and Bond Type Perception in Molecular Mechanical Calculations. *J. Mol. Graph. Model.* **2006**, *25* (2), 247–260.
- (25) Maingi, V.; Jain, V.; Bharatam, P. V.; Maiti, P. K. Dendrimer Building Toolkit: Model Building and Characterization of Various Dendrimer Architectures. *J. Comput. Chem.* **2012**, *33* (25), 1997–2011.
- (26) Wang, J.; Wolf, R. M.; Caldwell, J. W.; Kollman, P. A.; Case, D. A. Development and Testing of a General Amber Force Field. *J. Comput. Chem.* **2004**, *25* (9), 1157–1174.
- (27) Ewing, S. A.; Donor, M. T.; Wilson, J. W.; Prell, J. S. Collidoscope: An Improved Tool for Computing Collisional Cross-Sections with the Trajectory Method. *J. Am. Soc. Mass Spectrom.* **2017**, *28* (4), 587–596.
- (28) Roe, D. R.; Cheatham, T. E. PTRAJ and CPPTRAJ: Software for Processing and Analysis of Molecular Dynamics Trajectory Data. *J. Chem. Theory Comput.* **2013**, *9* (7), 3084–3095.
- (29) Accelrys Software Inc. Materials Studio v6.0.0. 2011.
- (30) Saucy, D. A.; Ude, S.; Lenggoro, I. W.; Fernandez De La Mora, J. Mass Analysis of Water-Soluble Polymers by Mobility Measurement of Charge-Reduced Ions Generated by Electrosprays. *Anal. Chem.* **2004**, *76* (4), 1045–1053.
- (31) Hogan, C. J.; Fernández De La Mora, J. Ion Mobility Measurements of Nondenatured 12–150 KDa Proteins and Protein Multimers by Tandem Differential Mobility Analysis-Mass Spectrometry (DMA-MS). *J. Am. Soc. Mass Spectrom.* **2011**, *22* (1), 158–172.
- (32) Müller, R.; Laschober, C.; Szymanski, W. W.; Allmaier, G. Determination of Molecular Weight, Particle Size, and Density of High Number Generation PAMAM Dendrimers Using MALDI-TOF-MS and NES-GEMMA. *Macromolecules* **2007**, *40* (15), 5599–5605.
- (33) Williams, T.; Kelley, C. Gnuplot 4.6. 2013.
- (34) Maiti, P. K.; Çağın, T.; Wang, G.; Goddard, W. A. Structure of PAMAM Dendrimers: Generations 1 through 11. *Macromolecules* **2004**, *37* (16), 6236–6254.
- (35) Sun, L.; Yang, L.; Zhang, Y. D.; Shi, Q.; Lu, R. F.; Deng, W. Q. Accurate van Der Waals Force Field for Gas Adsorption in Porous Materials. *J. Comput. Chem.* **2017**, *38* (23), 1991–1999.

For Table of Contents Use Only

HOW SPHERICAL ARE GASEOUS LOW CHARGED DENDRIMER IONS: A MOLECULAR DYNAMICS / ION MOBILITY STUDY.

Fabrice Saintmont^{a,b}, Julien De Winter^a, Fabien Chiro^c, Emilie Halin^a, Philippe Dugourd^d, Patrick Brocorens^b, Pascal Gerbaux^{a*}



Impact on the ion surface roughness on the gaseous ion density determined by ion mobility experiments: globular dendrimer ions as the case study.